Estimating thermal properties of phase change material from heat flux measurements

Elodie Courtois, Patrick Glouannec, Anthony Magueresse, Tahar Loulou

Estimating thermal properties of phase change material from heat flux measurements

Elodie Courtois, Patrick Glouannec, Anthony Magueresse and Tahar Loulou*

Université Bretagne Sud,

UMR CNRS 6027, IRDL

F-56321, Lorient, France

tahar.loulou@univ-ubs.fr

September 7, 2021

Abstract

An inverse analysis is applied to estimate the effective heat capacity and thermal conductivity of phase change material (PCM) as function of temperature. A sequential work in two distinct parts was adopted here which consists in the estimation of the thermal properties of the PCM in the solid and liquid states in a first step and completed by the characterization of the phase change in a second step. The effective heat capacity is judiciously parameterized as temperature dependent function to take into account the phase change phenomenon and its two solid and liquid phases. An experimental setup was built to collect the heat fluxes and temperatures histories around and inside a one dimensional sample of PCM. First the experimental data were used to estimate thermal conductivity and specific heat both at solid and liquid state and later combined with the developed inverse analysis to estimate the specific heat function over the phase change transition. Obtained results are compared to those obtained with the DSC facilities and an acceptable agreement between the two approaches is observed. The experiment was found to be well designed and the collected measurements trustworthy and complementary to handle this important estimation problem.

keywords = Latent heat; effective specific heat; PCM material; numerical simulation; experimental analysis; thermal conductivity; inverse analysis

Highlights

- Implementation of an enthalpy-based effective heat capacity.
- Estimation of thermophysical properties trough the solution of an inverse parameter problem.
- Obtained results are validated and compared to previously published experimental data.
- Building an experiment to characterise thermal behavior of PCM-mortar in close real use-conditions.

*Corresponding author

- Development of an experimental methodology to estimate thermal properties of PCM material.

1 Introduction

Phase change materials (PCMs) are substances that absorb or release heat quantity during melting or solidification transition respectively. This is the main reason for which such materials have received a great interest for many industrial and environmental applications such us: thermal storage, aircraft cabin temperature control, building thermal management, ... and are expected to play an important role in energy saving and offering ground-breaking reliable solutions to the challenges of energy transition in the future.

Two well established methods are extensively used to solve the moving boundary problem occurring in the PCMs under use, i.e. front tracking methods and fixed-domain methods [1, 2]. The later methods (known as enthalpy method) treat both the solid and liquid as one continuous medium and interface condition becomes implicit in a new form of the equations described by the enthalpy h, effective heat capacity c_p^e, apparent heat capacity c_p^a or heat generation term, etc [3–6]. In the enthalpy method, the latent and specific heat are combined into an effective or apparent heat capacity in the governing equation as proposed by Eyres et al. [7] to deal with variations of thermal properties with respect to temperature. The enthalpy method is simple compared to the others, most versatile and more convenient.

The effective/apparent specific heat capacity approximation is well spread and commonly used in the literature and research work dealing with casting, permafrost, thermal storage energy (TES), phase change material (PCM), ... This thermophysical characteristic (specific heat) plays a fundamental role in the heat transfer phenomenon and should be well known [3, 8]. In the PCM research field the approximation of specific heat during the phase change is still under enhancement and commonly used to simulate the release or the storage of thermal energy [9–27].

The DSC is the most used laboratory measurement to obtain the kinetic of melting/solidification of PCM samples. The limitations of the DSC are the very small sample size (lack of representation because the small used volume/mass), the influence of the test procedure on the results (heating rate, cooling rate) and especially failure for dynamic measurements with constant heating and cooling rate, where a slow rate is needed for PCMs unlikely the typical standards used in DSC analysis for other materials [16, 28, 29].

Another approach for estimating the thermophysical properties of materials is the solution of inverse heat conduction problems [30–33]. Such problems could be dealt by means of optimization methods including derivative and non-derivative methods [34]. In this case, the objective is to minimize the discrepancy between measured values (which can be temperature or/and heat flux) and calculated values based on the estimated properties. The advantage of this approach is that the measurements can be obtained from an experiment which closely reproduces the real conditions of use of a PCM in terms of thermal boundary conditions and geometry. Inverse problems are known to be ill-posed, i.e. under small variations of the input data the three conditions of existence, uniqueness and stability of the solution are not satisfied. The ill-posedness character is more difficult in the case of function estimation than the parameter estimation problem which is the case in this paper.

Derbal et al. [35] present an estimation of thermal conductivity and heat capacity on materials with constant properties. They proposed a procedure that can be potentially applied to in-situ measurements. The material to be characterized is placed between two layers of materials with known thermophysical properties. Thermocouple probes are placed at the different interfaces and record the variations in temperature when the whole multilayered body is subjected to temperature variations. In addition to thermal conductivity and heat capacity, Chaffar et al. [36] estimated also the surface film coefficient of a homogeneous panel by applying a heat flux and studying the response in terms of the temperature recorded by infrared thermography camera on the opposite surface.

Lachheb et al. [14, 37] proposed a method for estimating thermal conductivity, specific heat and thermal diffusivity of paraffin/graphite PCM composites from laboratory tests under controlled boundary conditions, but material properties were evaluated at room temperature and their dependency on temperature was hence not investigated. Thermal conductivity and specific heat as a function of temperature of PCM-concrete bricks subjected to controlled boundary conditions were estimated by Cheng et al. [13]. The temperature dependency was evaluated through the temperature segment method, which has the advantage of not requiring any a-priori knowledge on the specific heat function. However, the number of segments directly determines the number of variables in the optimization problem. Temperature-dependent thermal conductivity, heat capacity and thermal diffusivity were simultaneously estimated by Cui et al. [38], who proposed an approach based on the measurement of the temperature distribution within the material and subjected either to Dirichlet or Neumann boundary conditions. Prior information on the functional form of the thermal properties is not necessary.

This paper is devoted to the solution of a heat transfer problem involving phase change that is accompanied by either absorption (melting) or realise (solidification) of heat energy by using two kinds of thermal measurements, i.e. temperatures and heat fluxes. These measurements are collected by the means of well designed laboratory apparatus that enables PCM-mortar blocks to undergo any desired thermal cycles. The aim of the present work is to complete a previous published work [39] by presenting a methodology for estimating thermophysical properties of PCM incorporated in mortar. Identical cement based flat plates containing a volume fraction of PCM microcapsules (a volume fraction higher than 29% in this study against lower values in literature [? 40]) are used. Thermal characterization is carried out using measurements collected around the sample according the following steps: (1) measured temperatures and heat flux on the faces (boundaries) of the sample are used to calculate thermal liquid and solid conductivities and specific heats of the sample over specific periods which will be considered known for the next steps, (2) the kinetic of phase change (melting $\rightleftarrows$ solidification) is determined following the method presented by Joulin et al. [17] over different thermal cycles, (3) the effective specific heat is estimated thanks to the solution of an inverse problem during two stages: melting and solidification and then (4) a comparison between obtained results concludes this investigation work.

2 Experimental setup

A sketch of the experimental setup used to estimate the thermal properties of the PCM material is depicted in Fig. 1. The following two paragraphs present in details: (1) the specimen nature and elaboration, and (2) the main elements of the specimen holder.

2.1 Sample's elaboration

In the scope of this work, the studied material is a parallelepiped-shaped cement-mortar sample with a particular size of ($13 \times 13 \times 2.2\,cm^3$). This composite material is a mortar-matrix incorporating a Portland cement (containing exclusively clinker and gypsum), river sand with low absorption capacity, and microencapsulated paraffin. The mixture proportions, methodology to obtain desired volume fractions of the PCM in the composite, and the mixing procedure are detailed in reference [39]. Briefly a such typical procedure is described as follows: a certain amount of cement, sand and water are mixed during a moment. To limit the break-up of microencapsulated paraffin, it is added at the final step. Then, the mixture must be constantly agitated at very-low speed until the microencapsulated PCM homogeneously diffuse and then forms the PCM-mortar. The final mixture is then poured gently into a PVC-mold to reduce entrained air, slightly compressed and then allowed to stand in curing chamber (70% of relative humidity and $20 \pm 1\,^{o}C$) for 24 h.

Note that the accurate measurement of thermal properties requires a very smooth sample surface. The used selected microencapsulated PCM is the n-octadecane ($C_{18}H_{38}$) supplied by Microtek laboratories: $MPCM-28$. The microcapsules have a spherical shape with a diameter ranging between 17 and 20 μm. This phase change material has a relatively high latent heat storage capacity (about $180 \sim 195\,J/g$) and leakage proof in the liquid phase. The microcapsules have a spherical shape with a diameter ranging between 17 and 20 μm and contains in the core of microcapsules a latent heat storage material made from a special paraffin wax mixture. The latter is coated with a thin layer ($e = 0.1 \sim 0.2 \mu m$) of polymer shell (15% by weight). According to the supplier, the wall is a melamine-formaldehyde and is chemically inert in concrete and cement. The melting point of the microencapsulated PCM, as provided by suppliers, is around $28\,^{o}C$.

During the casting process a thin K-type thermocouple (diameter of $125 \mu m$) is stretched approximately in the half thickness of the sample. This thermocouple allows the collect of temperature history inside the sample when it undergoes any heating or cooling effect on its sides. Due to the experimental uncertainties, its position remains unknown during the whole work. The precise spatial position of this sensor will be determined once all the planned tests were accomplished and then the sample can be destroyed.

2.2 Experimental device

The proposed test bench, assimilated to a flat plate, provides temperature and heat flux measurements at the material borders. Indeed and as shown in figure 1, the sample is located between two horizontal heat exchangers fueled by two thermo-regulated baths. To increase the contact quality and to reduce the thermal contact resistance effect between the sample and the heat exchangers, two very thin aluminum foils are interleaved between the heat exchangers and the sample (green color in the figure 1). Indeed, the high thermal conductivity of aluminum and its softness reduces considerably the trapped air in the roughness and its effects on both contact interfaces. The thermo-regulated baths supply the two exchangers by two heat-carrying fluids at different regulated temperatures which ensure a thermal gradient inside the specimen thickness. In this way, the two baths allow a fine regulation of the injected fluid temperature with a precision of approximately $0.1 \sim 0.5\,^{o}C$.

One fast response thin-film heat flux sensors (type $layer$) and one thermocouple (type K, diameter

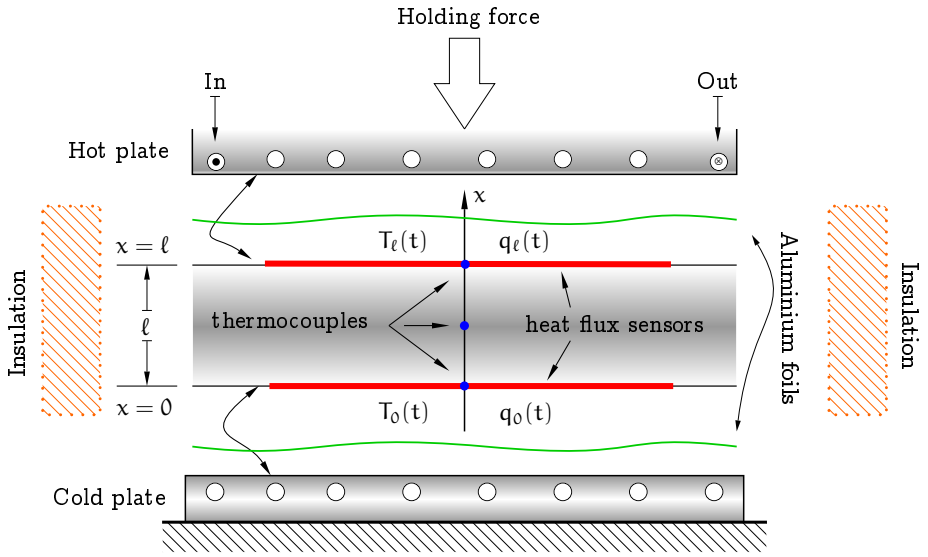

Figure 1: Experimental setup, coordinates, boundary conditions and geometry of the model.

125 µm) are placed on each side of the specimen, i.e. $x = 0$ and $x = \ell$ to measure heat flux and temperature of each surface. Arranged in sandwich form, heat flux sensors and PCM simple are maintained in place by the use of a slightly tightened pneumatic cylinder. Regulated air cylinder provides power to gently move the top side, urging its position into the desired contact pressure so that the contact between surfaces is thermally good. However care should be taken to see that the applied force does not change neither the density of the sample material nor the thickness of flux meters which is approximately 0.2 mm. The flux meter sensitivity is approximately $65\,\mu V/W/m^2$ for a sensor having a square active surface area of $10 \times 10\,cm^2$ (red color in the figure 1). The various sensors are connected to a computer which runs a Labview® program adapted to collect both heat fluxes and temperature measurements and monitor the thermo-regulated baths. Simultaneous measurements of temperatures and heat fluxes are recorded with regular and adjustable time steps. The measurement errors of temperature and heat flux are respectively $\pm 0.25\,°C$ and $\pm 0.01\,W/m^2$. The lateral side faces are covered with foam insulation to reduces multidimensional heat transfer to a $1-D$ problem. Figure 2 displays all measurements collected by the developed experimental setup presented above.

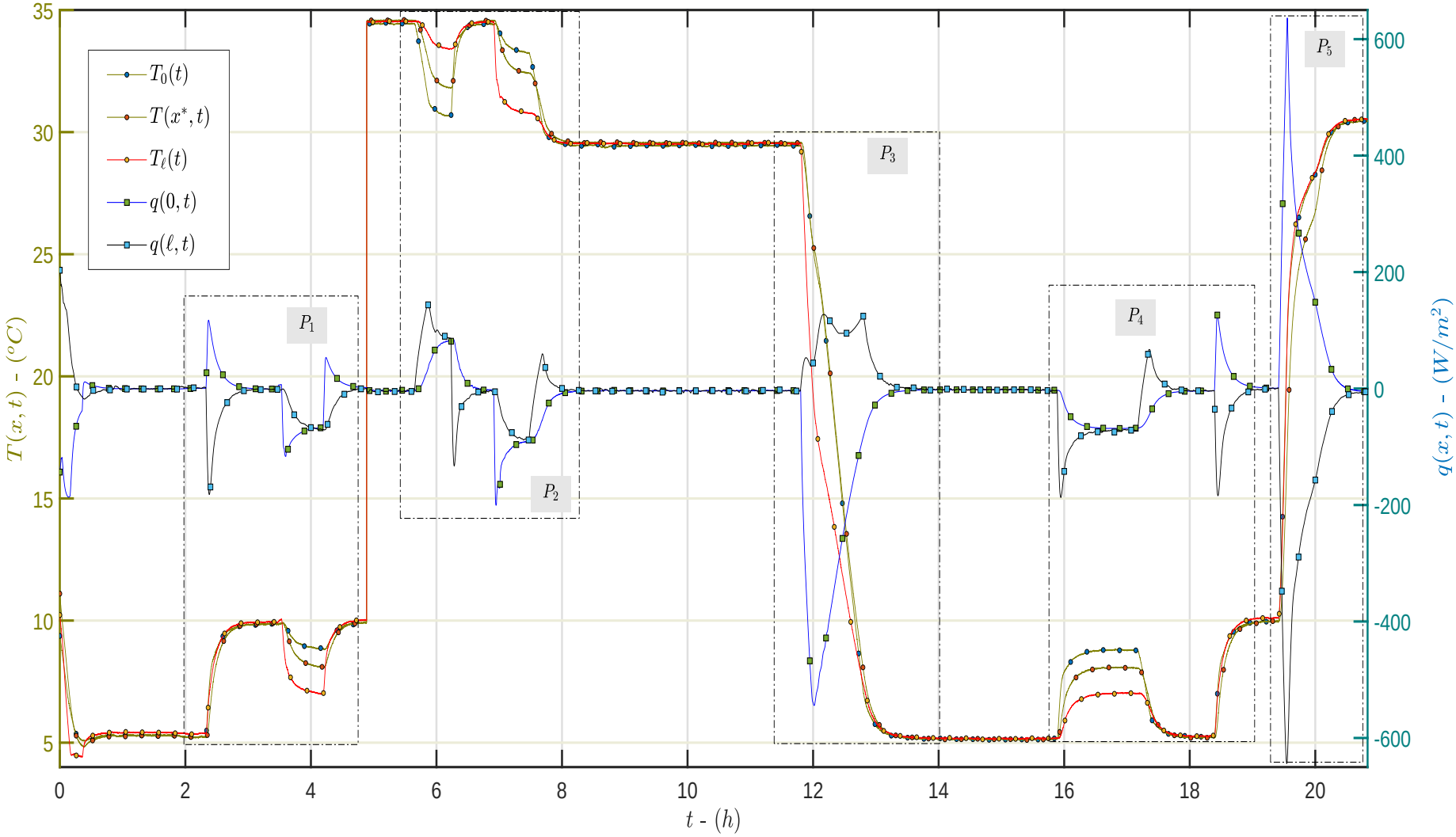

Figure 2: Measured temperatures and heat fluxes on both sides of the sample. $T(x^*, t)$ represents the temperature measurement inside the sample at $x^* \sim 0.013$ m. Dotted regions P_4 and P_5 represent the periods over which the PCM undergoes the state change: solid $\rightleftarrows$ liquid. Each period $P_1, \ldots, P_5$ will be used separately in estimating the different thermophysical properties of the PCM.

3 Heat transfer problem formulation

As detailed previously, the sample used in the experiment is a mixture between a classic building cement and very small particles of microencapsulated PCM. However, despite these inclusions the obtained mortar may still be considered as a homogeneous and isotropic medium. Therefore, to reproduce the thermal behavior of this type of material, the composite sample may be described via average thermophysical properties ($c(T)$, $k(T)$, $h(T)$, ...) that depend continuously on temperature.

The model adopted for this work is based on one-dimensional macroscopic nonlinear heat conduction problem. The slab thickness is ℓ and its initial temperature distribution is denoted $g(x)$. The slab can be heated or cooled on its surfaces $x = 0$ and $x = \ell$ independently. Figure 1 shows the schematic shape of the physical problem under picture and the principle of the built experimental device. Using the enthalpy formulation, the problem can be expressed in the following form [1]:

$$\rho\frac{\partial h}{\partial t} = \frac{\partial}{\partial x}\left(k(T)\frac{\partial T}{\partial x}\right) \qquad 0 < x < \ell \qquad t > 0 \tag{1}$$

with the following boundary conditions :

$$-\,k(T)\frac{\partial T}{\partial x} = h_0\Big[T_0(t) - T(0,t)\Big] \qquad x = 0 \quad t > 0 \tag{2}$$

$$+\,k(T)\frac{\partial T}{\partial x} = h_\ell\Big[T_\ell(t) - T(\ell,t)\Big] \qquad x = \ell \quad t > 0 \tag{3}$$

$$T(x,t) = g(x) \qquad 0 \leqslant x \leqslant \ell \qquad t = 0 \tag{4}$$

Temperatures $T_0(t)$ and $T_\ell(t)$ designate the measured temperatures on both sides $x = 0$ and $x = \ell$ of the sample. They represent approximately the temperature of the fluids carried-out from the thermoregulated baths. Thermal contact conductances between the sample sides and the exchangers are modeled by thermal conductances h_0 and h_ℓ.

If the functions $g(x)$, $h(T)$, $k(T)$ and the constants h_0 and h_ℓ are known, the above heat conduction problem may be solved by any numerical method. In this case we are dealing with the solution of the direct problem to get the temperature field in the slab. In the remain part of the paper, the finite difference method [41] is used to obtain the temperature field in the slab.

The temperature dependent conductivity $k(T)$ is mixture between the solid and liquid phases, i.e. function of phase change fraction, defined as:

$$k = (1 - f)k_s + fk_l \tag{5}$$

Also, the enthalpy function $h(T)$ is mixture expressed as:

$$h(T) = (1 - f)\int_{T_r}^{T} c_s\,d\zeta + f\int_{T_r}^{T} c_l\,d\zeta + Lf \tag{6}$$

In the above equations, the subscript s and l refer to solid and liquid phases, respectively. T_r is an arbitrary reference temperature, ρ is the density of PCM, c the specific heat, L is the latent heat of melting/freezing, and f is the local liquid volume fraction. Equation (1) can be more conveniently expressed in terms of temperature variable as:

$$\rho c\frac{\partial T}{\partial t} = \frac{\partial}{\partial x}\left(k(T)\frac{\partial T}{\partial x}\right) + S \qquad 0 < x < \ell \qquad t > 0 \tag{7}$$

where the parameter c is defined as:

$$c = (1 - f)c_s + fc_l \tag{8}$$

which represents a mixture of solid and liquid specific heat. Then the source term S appearing in equation (7) is defined as:

$$S = -\delta H \frac{\partial f}{\partial t} \tag{9}$$

where, and assuming a reference temperature of $T_r = 0$,

$$\delta H = \rho(c_l - c_s)T + \rho L \tag{10}$$

The new governing equation (7) contains two unknowns the liquid fraction f and temperature T. The liquid fraction f can be a function of many variables but usually it is assumed to be a function of temperature alone, and written as

$$f = F(T) \tag{11}$$

with different possible continuous shapes such as : linear approximation, sigmoid function, power law and so on. All of these functions are varying from 0 to 1 during the melting transition case over a range of temperature ΔT for non-isothermal problem. With this approach, the fluid fraction can be linearized and the equation of energy can be solved iteratively with temperature.

Commonly used linearizing models of the liquid fraction function $F(T)$ for non-isothermal phase transition materials are [3, 8, 42, 43] :

$$F(T) = \begin{cases} \dfrac{T - T_s}{T_l - T_s}, & \text{linear variation;} \\ \dfrac{1}{2}\left[1 + \operatorname{erf}\left(4\dfrac{T - T_m}{T_l - T_s}\right)\right], & \text{error function;} \\ \left(\dfrac{T - T_s}{T_l - T_s}\right)^n, & \text{power law.} \end{cases} \tag{12}$$

In these cases, the equivalent solidus and liquidus temperatures are defined such as $T_s = T_m - \Delta T/2$ and $T_l = T_m + \Delta T/2$. Figure (3) shows the three shapes of $F(T)$ given in equation (12) The linear approximation, presented previously, is extensively used and is cited only as a reminder and will not be used in the rest of the article.

Thermal conductivity and specific heat are supposed to be constant in the solid and liquid regions respectively (k_s and k_l, c_s and c_l) and their temperature-dependent variations are occurring mainly during the solidification/melting transition through the locally change of the liquid fraction f. Finally the initial formulation of the problem is reduced to use equation (7) with the boundary and initiale conditions (2), (3) and (4). General source-based method developed by Voller and Swaminathan [42, 44] with finite volume approach is used in the solution of the above phase change problem. Appendix A presents a comparison between the results of enthalpy method and the known Neumann analytical solution.

The phase change occurring in the PCM will be totaly defined and controlled when any thermal load is applied on its surfaces if the parameters k_s, k_l, c_s, c_l, L, and ΔT are precisely known. The constraints of the experiment detailed above introduce two more unknown parameters that are h_0 and h_ℓ reflecting

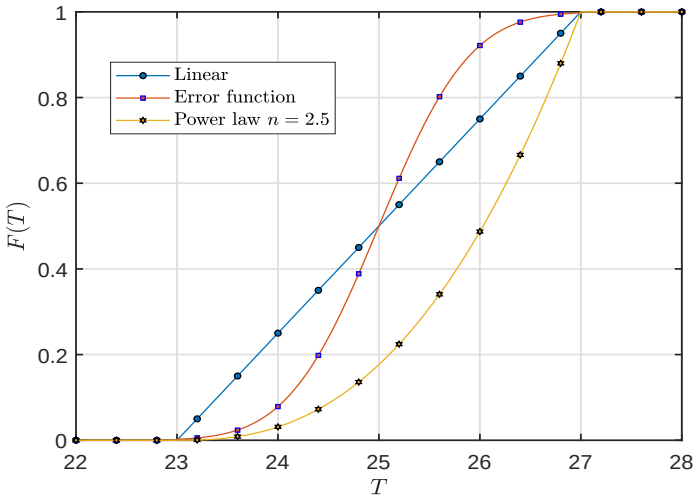

Figure 3: Liquid fraction approximation F(T) with linear, error function and power law ($n = 2.5$). Melting temperature and transition range are taken as $T_m = 25\,^{\circ}C$ and $\Delta T = 4\,^{\circ}C$

the imperfection of the contact between the sample and the two heating walls. All these unknowns can be recast in the following vector of 9 components $\boldsymbol{\beta} = \left[k_s, k_l, c_s, c_l, L, T_m, \Delta T, h_0, h_\ell,\right]^\top$. In the case of power law model of F(T) a tenth component is added to this vector representing the exponent of the law n.

4 Parameter estimation

The basic idea of the inverse problem considered in this study is regarded as a parameter estimation problem. It is about determining the vector of parameters β that minimizes a fitness function $S(\beta)$ that corresponds to the gap between the measured heat fluxes $p(x_i, t_j)$ and the mathematical model output $q(x_i, t_j)$ and to improve estimated parameters until the mathematical model output is sufficiently close to the measurements as written in the following equation:

$$S(\beta) = \sum_{i=1}^{N_s} \sum_{j=1}^{N_t} \left[p(x_i, t_j) - q(x_i, t_j)\right]^2 \tag{13}$$

where N_s is the number of heat flux sensors installed in the slab and N_t the total number of measurements over the whole experimental time t_f. To minimize this fitness function there are many methods, among them we mention the gradient methods which are largely used by many researchers in different science and engineering domains. Although these techniques are well developed, they maintain significant drawbacks. Their principle requires the evaluation of the derivatives of the fitness function $S(\beta)$ by differentiating equation (13) with respect to each of the unknown parameters β_k, i.e. $k = 1, \ldots N_p$, and then setting the resulting expression equal to zero yielding to the following set of algebraic equations:

$$-2 \sum_{i=1}^{N_s} \sum_{j=1}^{N_t} \frac{\partial q(x_i, t_j)}{\partial \beta_k} \left[p(x_i, t_j) - q(x_i, t_j)\right] = 0, \qquad k = 1, \ldots N_p \tag{14}$$

where N_p is the number of parameters being sought-after. From their principle, the gradient methods can be applicable only for derivable functions. Furthermore, employing gradient search methods mechanism need to start from an initial guessed solution near to the exact solution. In these approaches, the use

of a bad starting point may result in the solution getting trapped in a local optimum [30]. In the present work, the Levenberg-Marquardt method, built-in the toolbox Optimization of MATLAB is used to minimize the function $S(\beta)$ [45–48].

The idea of estimating the 9 components of vector β at once can present some difficulties to overcome and therefore is delayed for future work. To facilitate the estimation of these unknowns the following methodology is adopted in this paper and it consists in three sequential steps: (1) estimating the components k_s, c_s, h_0 and h_ℓ during the solid stage, (2) estimating k_l, c_l, h_0, h_ℓ during the liquid phase and then (3) estimating the remain parts of vector β, i.e. L, T_m, ΔT, h_0, h_ℓ and n. To achieve efficiently and correctly this methodology the applied thermal boundary conditions on the specimen are specified differently between (1) the solid phase, and (2) the liquid phase and then (3) the melting/freezing transition by an optimal variation. By doing so the required conditions for estimating the parameters sought in each of the three steps are gathered and satisfied.

Concretely the applied boundary conditions for each step (P_i, $i = 1 \ldots 5$) can be better viewed in figure 2 displaying the collected experimental data. The measurements of periods P_1 and P_4 are intended to estimate the parameters of the solid phase because the temperature variation range is largely below the melting temperature of the PCM material which is found to be around $26\,^{o}C$. As for period P_2, this exhibits variation ranges above the melting temperature of the PCM and is consequently used to estimate the properties of the liquid phase. And finally, the measurements of periods P_3 and P_5 are intended for the estimation of the thermophysical parameters of the PCM during the solid-liquid transition or vice versa. It is noted that over each of the periods, cited above, that the specimen is subjected to a precise thermal gradient through its thickness in order to maximize the sensitivities of all parameters actually sought and to ensure a good and reproducible estimate.

The parameter estimation presented in this work is slightly different than those observed in the literature in the sense that the objective function $S(\beta)$ to be minimized is heat-flux based measurement instead of commonly measured temperature based function [30–32]. Very little things have been said about the feasibility of estimating thermal characteristics with heat flux data in specialized literature. The use of heat flux measurements in inverse problems is different from that of temperatures and therefore needs to be carefully considered and investigated.

5 Sensitivity analysis

It is well known that before any estimation procedure for several parameters, a carefully sensitivity analysis is required to quantify the importance and weight of each parameter and if there is any correlation between them. The finite difference method is used to compute all normalized sensitivity coefficients. To check the quality of obtained measurements, the boundary conditions applied in the sensitivity analysis are shown in figure 2 for each considered period (P_1 solid, P_2 liquid, P_4 solid and P_5 solid/liquid transition). They correspond to measured temperatures at the location $x = 0$ and $x = \ell$ for each considered period, i.e. $T_0(t)$ and $T_\ell(t)$. The numerical values of the vector components of β used to perform the sensitivity analysis are taken as $\left[1.10, 0.95, 1050, 1075, 19500, 25.50, 6.25, 300, 300, 2.5\right]^{\top}$. The thickness of the solid is equal to $0.0218\,m$. The analysis time is taken equal to the experiment time for each considered period.

At the sensor position x and time t, the normalized heat flux sensitivity coefficient, with respect to the

parameter β_k is defined by:

$$X_k(x,t) = \beta_k \frac{q(x,t,\beta_1,\ldots,\beta_k+\Delta\beta_k,\ldots,\beta_{n_p}) - q(x,t,\beta_1,\ldots,\beta_k-\Delta\beta_k,\ldots,\beta_{n_p})}{2\Delta\beta_k} \qquad (15)$$

The quantity $\Delta\beta_k$ is a small perturbation of the parameter β_k taken equal to $10^{-4} \sim 10^{-5}$ for all parameters. N_p is the number of parameters. With this definition the coefficients $X_k(x,t)$ have the units of heat flux (W/m^2) and can compared to each other.

The simultaneous identification of set of parameters using any based gradient method is feasible only if all parameters are uncorrelated during the experiment time. The correlation among all parameters is obtained by computing the off-diagonal elements of the correlation matrix [30] and analyzing the behavior of all sensitivity coefficients once plotted as time function.

The same insight regarding the sensitivity coefficient analysis can be gained graphically. Indeed, the correlation between the components of the vector β is better viewed when the variation of each sensitivity coefficient is plotted individually as function of time. Figures 4, 5 and 6 display all sensitivity coefficients for each considered period: solid P_1, liquid P_2 and solid/liquid transition P_5. These sensitivities are computed for heat flux measurements located on both sides of the PCM sample, i.e. $x = 0$ and $x = \ell$. In what follows, each period is treated separately.

Solid and liquid phases. The solid and liquid phases are analyzed separately by using the measurements of periods P_1 and P_2 respectively. The graphical inspection of all figures (4)-(5) shows that all parameters are uncorrelated and their sensitivity coefficients present almost the same time-variation for both sensor locations for each phase, i.e. solid and liquid. Some sensitivity coefficients show more or less noised curves attributed to two things : (1) the use experimental data as boundary conditions in solving the related heat conduction problem and (2) the differentiation operation in computing the sensitivity coefficients, equation (15). It is well known that a differentiation operation amplifies the noise of measurement.

All normalized sensitivity coefficients are of the same order displaying an alternation between negative and positive values. They present the same amplitude of heat flux variation equivalent to the interval $[-60,\ +120\,W/m^2]$. The highest amplitude variation is observed with specific heat coefficients X_c for solid and liquid phases, figures 4b and 5b. Their magnitudes are the same of measured heat fluxes for both periods P_1 and P_2. This is much better than having the sensitivity coefficients very much smaller than the heat flux range. This reflects a good sensitivity of all parameters to the applied boundary conditions for the sensor installed at $x = 0$ and $x = \ell$ indicating that this location contains an important amount of information for estimating an important number of components of vector $\boldsymbol{\beta}$. Hence the sensitivities are not linearly dependent over the whole considered time domains (P_1 and P_2), no difficulty would be anticipated in estimating the six parameters $[k_s, c_s, k_l, c_l, h_0, h_\ell]$ and the experiment is found to be well designed.

Tables 1-a and 1-b show the correlation matrix of the parameters sought in the solid and liquid regions. The absolute values of the non-diagonal elements of the two matrices are less than 0.9 and consequently reflect the non-correlation between the different parameters sought in this case and leading to a feasible simultaneous and unique estimation of all parameters by using heat flux measurements.

Phase change interval. Here the sensitivity coefficients of the phase change period P_5, displayed in figure 2, are computed and analyzed for error function and power law models, see equation (12). The applied boundary conditions on the PCM sample are those displayed in figure 2 over period P_5. The sensitivity

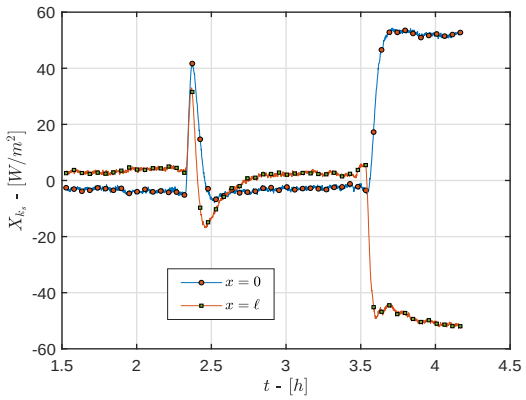

(a) Thermal conductivity k_s

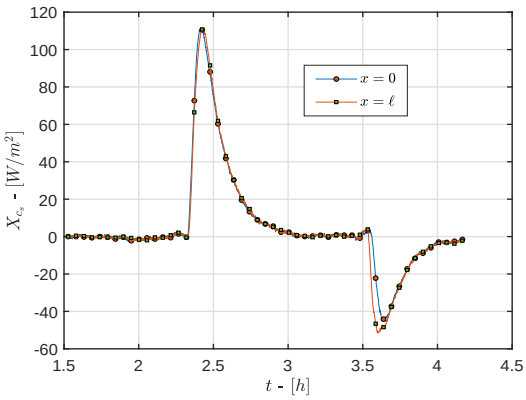

(b) Specific heat c_s

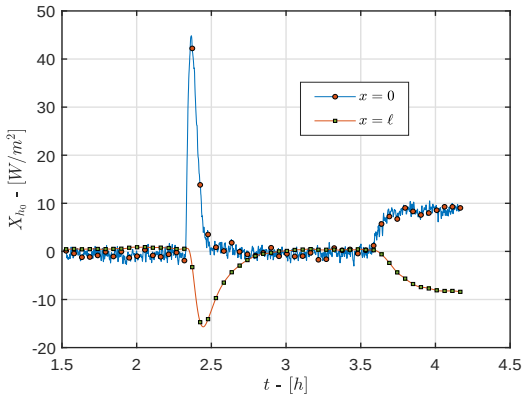

(c) Thermal conductance h_0

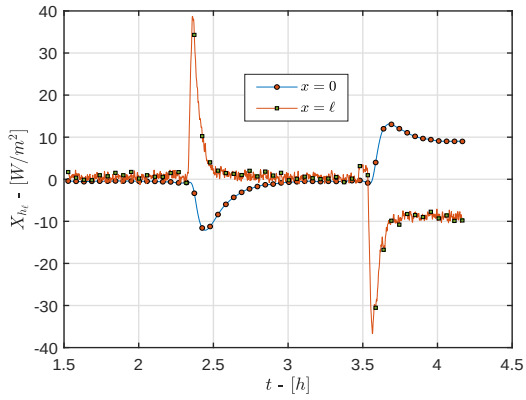

(d) Thermal conductance h_ℓ

Figure 4: Normalized sensitivities coefficients of estimated parameters over period P_1 (solid phase).

	k_s	c_s	h_0	h_ℓ
k_s	1	0.037453	0.654166	0.735074
c_s		1	−0.027880	0.075701
h_0			1	0.185108
h_ℓ				1

(a) Solid phase

	k_l	c_l	h_0	h_ℓ
k_l	1	0.034715	0.755722	0.819843
c_l		1	0.138160	−0.014542
h_0			1	0.437201
h_ℓ				1

(b) Liquid phase

Table 1: Correlation matrix for unknowns parameters of solid and liquid phases

coefficients for both models (error function and power law) are shown in figure 6 and it concerns latent heat L, melting temperature T_m, temperature range over which the phase change is taking place α (i.e. $\alpha = \Delta T/2$), and both thermal conductances h_0 and h_ℓ. Figure 6 clearly shows the absence of correlation between the searched parameters over this period for both models. These sensitivities are high and almost of the same order of magnitude of applied boundary conditions heat fluxes. For X_L, X_{T_m} and X_α the location of the sensors does not seem to affect the sensitivities and no difference is observed between the two positions $x = 0$ and $x = \ell$. The coefficient X_{T_m} shows the highest amplitude of variation between two extreme values, negative at the beginning and a positive towards the end of the transition period. Its estimation should not encounter any difficulties and should be the most precise among all unknown parameters. Due to lack of space, the variation of the sensitivity coefficient of power

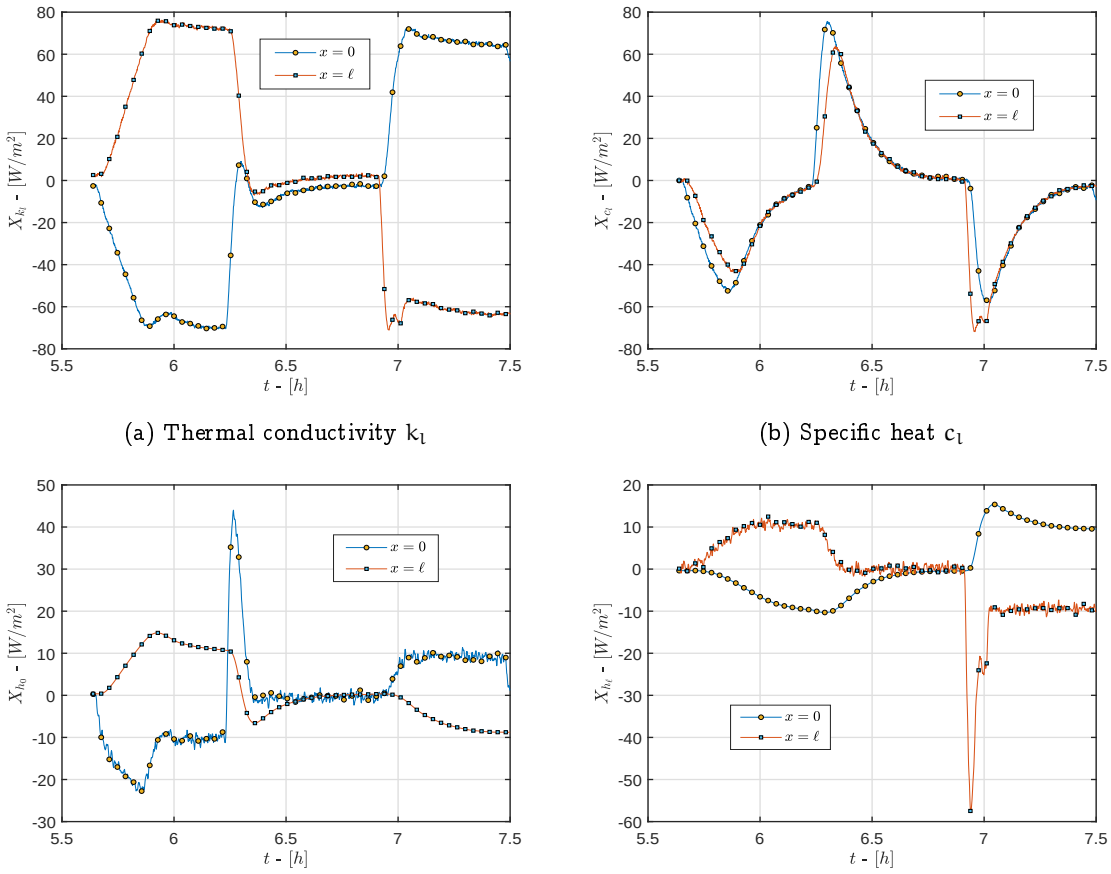

(a) Thermal conductivity k_l

(b) Specific heat c_l

(c) Thermal conductance h_0

(d) Thermal conductance h_ℓ

Figure 5: Normalized sensitivities coefficients of estimated parameters over period P_2 (liquid phase).

law model X_n is not shown here. It exhibits substantially the same variation as that of the melting temperature without showing the slightest correlation with it.

(a) Error function model

	L	T_m	α	h_0	h_ℓ
L	1	−0.14431	−0.54867	−0.18676	−0.17897
T_m		1	−0.17588	−0.31842	−0.33166
α			1	0.20290	0.23603
h_0				1	−0.50910
h_ℓ					1

(b) Power law model

	L	T_m	α	h_0	h_ℓ	n
L	1	−0.75764	−0.60985	−0.22484	−0.20978	−0.36622
T_m		1	−0.05468	0.17262	0.14488	0.86547
α			1	0.13805	0.15733	−0.49123
h_0				1	−0.65786	0.05939
h_ℓ					1	0.03569

Table 2: Correlation matrix for unknowns parameters of solid/liquid transition

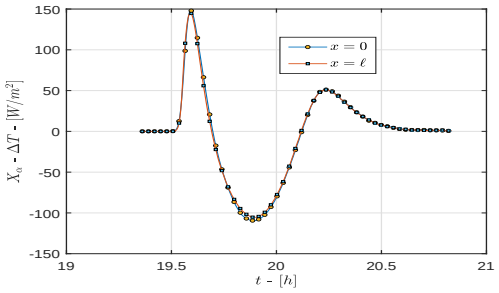

(a) Temperature range of phase change (ΔT)

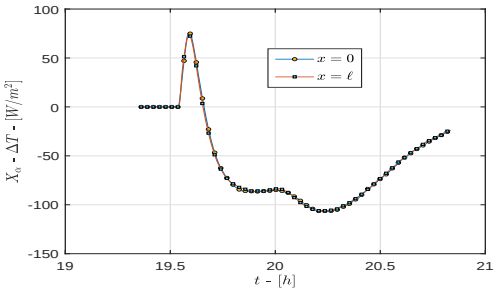

(b) Temperature range of phase change (ΔT)

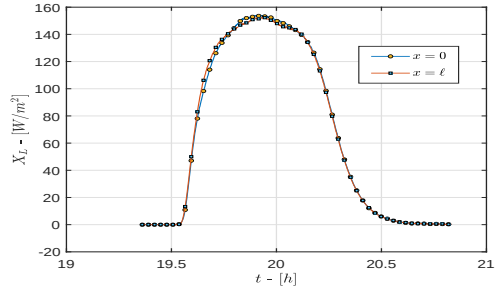

(c) Latent heat L

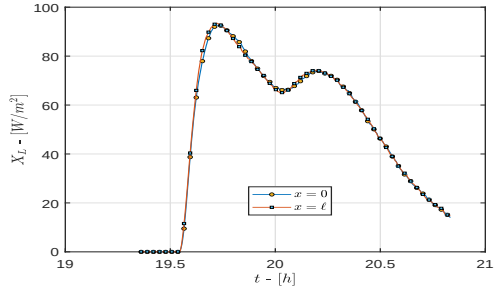

(d) Latent heat L

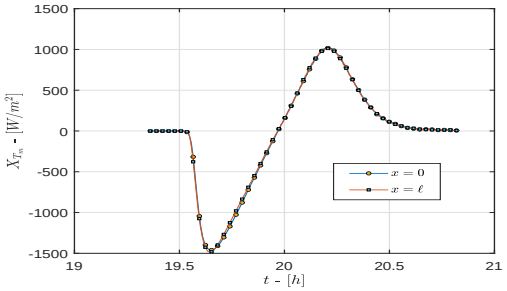

(e) Melting temperature T_m

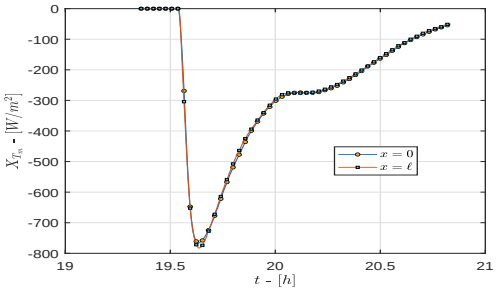

(f) Melting temperature T_m

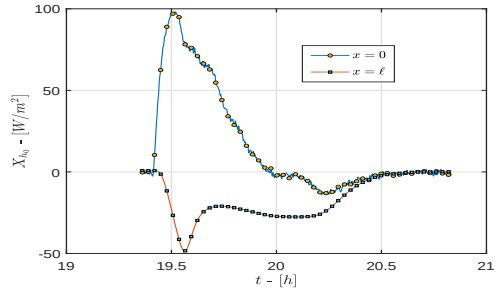

(g) Thermal conductance h_0

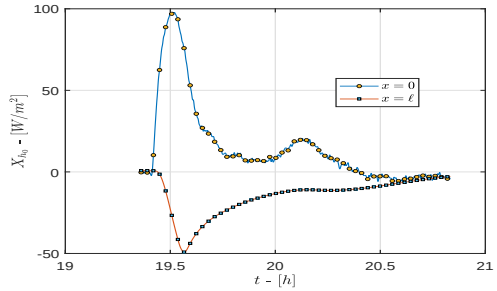

(h) Thermal conductance h_0

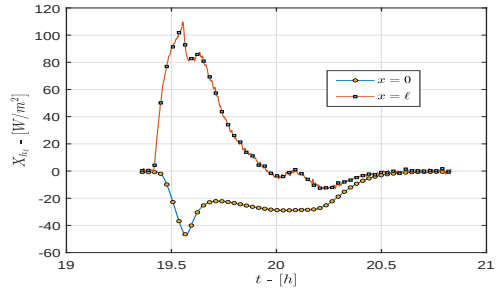

(i) Thermal conductance h_ℓ

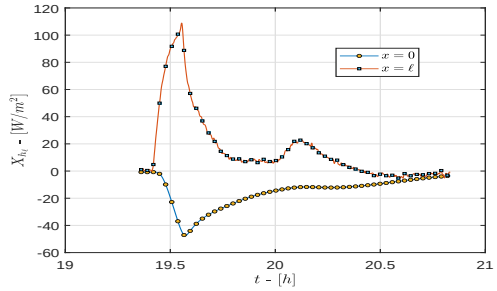

(j) Thermal conductance h_ℓ

Figure 6: Normalized sensitivities coefficients of unknown parameters over freezing/melting period P_5 for both fitting models : error function (left figures) and power law (right figures).

6 Experimental results processing

First the experimental conditions of the work are described. The sample is subjected to a series of thermal loads changing the PCM from the solid state to the liquid state and vice versa. Applied heat boundary conditions and obtained measurements (temperatures and heat fluxes) are displayed in figure 2. On a total time of more than 20 hours of experience, only the most interesting variations thermal loads will be used in the estimation of the desired parameters. The periods of interest are labeled P_1, P_2, P_3, P_4 and P_5 as shown in figure 2.

6.1 Solid and liquid phases

Initially the sample was at the temperature of 5 °C. Then the sample is heated until approximately 10 °C and maintained at this temperature for while to reach a steady state. Thereafter the plate temperatures (thermoregulated baths) are lowered a few degrees to create a temperature drop in the sample. These boundary temperature variations are intended to create enough beneficial information to allow a better estimation of parameters sought in the solid phase. This period is named P_1. Almost the same temperature variation is resumed over period P_4. Since the experiment conditions are identical between P_1 and P_4, the two experiments should give the same results for the solid phase.

Heat flux measurements obtained over period P_1 and P_4 are used to estimate the components k_s, c_s, h_0 and h_ℓ of vector β through the minimisation of least square criterion given in equation 13. Recorded temperatures of thermoregulated baths $T_0(t)$, $T_\ell(t)$ are used as boundary conditions in equations 2 and 3. Estimated results of these 2 periods and their confidents intervals are shown in table 3. As expected, both periods produce the same results attesting a good reproducibility of this experiment.

Parameter	k_s	c_s	h_0	h_ℓ
Units	$W.m^{-1}.K^{-1}$	$J.kg^{-1}.K^{-1}$	$W.m^{-2}.K^{-1}$	$W.m^{-2}.K^{-1}$
Period P_1	1.113 ± 0.017	1066 ± 6.35	452 ± 25.2	205 ± 6.50
Period P_4	1.166 ± 0.014	1061 ± 5.23	451 ± 18.80	219 ± 7.07
Mean value	1.140 ± 0.015	1063 ± 5.79	451 ± 22.0	212 ± 6.78

Table 3: Estimated parameters of solid phase with theirs confidence intervals over P_1 and P_4 periods

In the second period P_2, the walls of the sample have undergone a double temperature variation between 35 °C and 30 °C respectively starting from a steady state in each case. These temperature variations are intended to be used to identify liquid thermophysical properties of the PCM sample, i.e k_l, c_l and thermal conductances h_0 and h_ℓ. Estimated parameters and their confidences intervals over period P_2 are displayed in table 4.

Parameter	k_l	c_l	h_0	h_ℓ
Units	$W.m^{-1}.K^{-1}$	$J.kg^{-1}.K^{-1}$	$W.m^{-2}.K^{-1}$	$W.m^{-2}.K^{-1}$
Period P_2	0.837 ± 0.010	1117 ± 11	492 ± 36	499 ± 41

Table 4: Estimated parameters of liquid phase with theirs confidence intervals. Period P_2

A comparison between table 3 and 4 shows a slightly difference between the solid and liquid values of

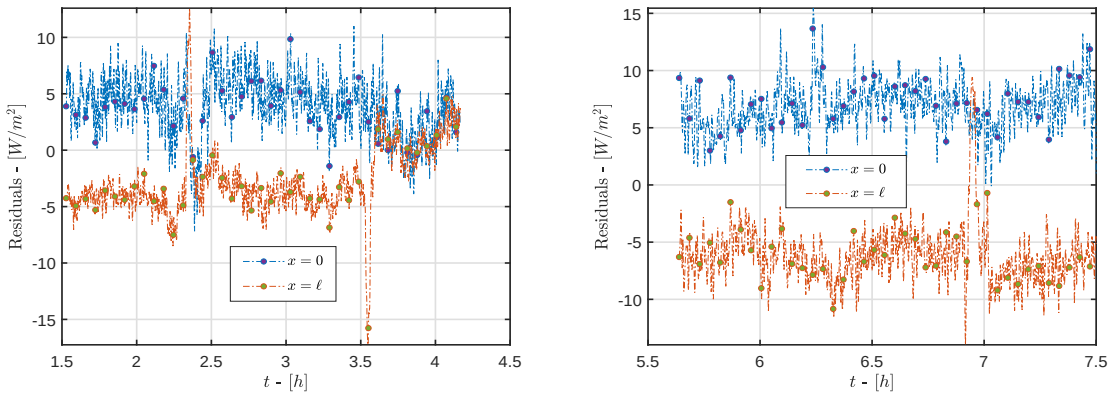

(a) Solid phase P_1 (b) Liquid phase P_2

Figure 7: Heat flux residuals over periods P_1 (solid) and P_2 (liquid)

thermophysical properties of PCM sample. For both phases, the recovered parameters are in agreement with those of the literature [17]. Thermal conductance h_0 ($x = 0$) is quasi-equivalent between both situations P_1 and P_2. Meanwhile there is a substantial difference between P_1 and P_2 for h_ℓ where its value is doubled for liquid case. Unfortunately only one period (i.e. P_2) when the PCM is totally liquid is available through this experiment which will prevent from confirming or invalidating the value of thermal conductance at $x = \ell$.

Figure 7 shows the heat flux residuals for both solid and liquid phases P_1 and P_2. The residuals are weak in comparison with the heat flux amplitude and of the same order of magnitude for both periods. However, the residuals are not distributed uniformly around the zero mean value. In fact, they are positive for the sensor located at $x = 0$ and negative for the sensor located at $x = \ell$ over the whole period P_1. The same observation can be drawn from the liquid case too (period P_2).

6.2 Phase change transition

In the remain part of the paper, gathered measurements are used to deal the estimation of parameters characterising the phase change (solid $\rightleftarrows$ liquid) according two models: error function and power law. From figure 2, unfortunately only the transition from solid to liquid can be investigated thanks to measurements of period P_5. Indeed, over period P_3, the heat flux measurement located at $x = \ell$ failed and cannot be utilized.

Starting from an initial constant temperature distribution around 10 °C, the sample is heated simultaneously on its both boundaries $x = 0$ and $x = \ell$ to reach the temperature level of $32 \sim 33$ °C. Nominated P_5, over this period the PCM changes from the solid to the liquid state as it crosses its melting temperature. The transition can be noted on the time evolution of measured temperatures as displayed in figure 2. Over period P_5, the slow heat diffusion in the sample creates a temperature gradient between its faces and its core which is well illustrated by the time evolution of measurement of the sensor installed in the middle of the PCM sample, see measured values of $T(x^*, t)$.

Measurements of period P_5 are used to estimate the missing parameters of error function and power law models, i.e. latent heat L, melting temperature T_m, temperature phase change interval α ($\Delta T/2$), h_0 and h_ℓ for error function model and the same components in addition to the power coefficient n for the

power law model. During period P_5, the parameters k_s, k_l, c_s, c_l, estimated previously are supposed to be known and used for the computation.

Parameter	α	T_m	L	h_0	h_l	n
Units	°C	°C	J/kg	$W/m^2.K$	$W/m^2.K$	–
Power law	4.66 ± 0.03	23.29 ± 0.10	18528 ± 155	3022 ± 723	688 ± 45	2.50 ± 0.03
Error function	6.26 ± 0.11	25.63 ± 0.04	19490 ± 225	1941 ± 448	588 ± 47	–

Table 5: Summarized estimated parameters of both models and their confidence intervals

Table 5 summarizes the estimated parameters and their confidence intervals for the phase change transition for both used models and appreciable differences are observed between them. Obtained thermal contact values are different and more important than those computed previously in the solid and liquid phases. Estimated parameters can now be used in computing enthalpy as a function of temperature. The enthalpy of PCM as function of temperature is graphed in figure 9.

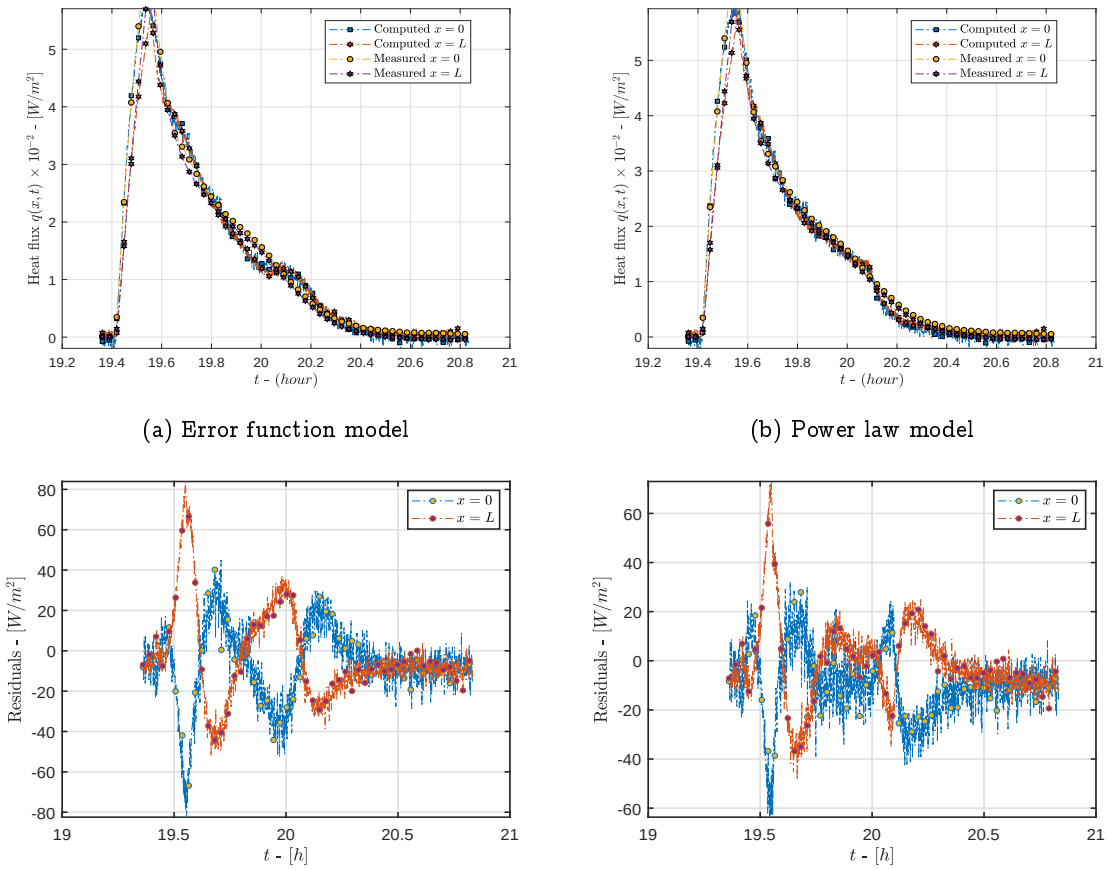

(a) Error function model

(b) Power law model

(c) Error function model

(d) Power law model

Figure 8: Comparison between computed and measured heat fluxes and heat flux residuals over periods P_5 for both used models

Figure 8 displays the heat flux residuals obtained after the parameter estimation of both developed models. The residuals exhibit the same behaviour, are more pronounced for the error function model

and are not well spread around the mean zero value as expected reflecting a deficit of the two models used in the phase change modeling. The mean values of residuals are different than zero for heat flux and are relatively very small in comparison with the heat flux rises $q_0(t)$ and $q_\ell(t)$ during the melting period P_5. The magnitude of the heat flux residuals is approximately $130\,W/m^2$ for power law model and $160\,W/m^2$ for error function model. These values remain high with respect to expected results. The residuals are still important reflecting a weak parameters estimation and non total adequation of developed models in this case. Better and more efficient approximation between enthalpie and temperature $(H-T)$ must be sought for this important problem.

The comparison with measurements of differential scanning calorimeter Micro DS3 of SETARAM® is not objective but just presented as an additional information. Indeed the measurement obtained with DSC facility is not representative of the sample because of the very low mass used in this kind of experiment, i.e. the sample volume is very small to be considered as representative of homogeneous material. Concretely in the present experiment, the mass of the PCM sample is about 0.8 kg while the one used in DSC apparatus is only few milligrams. The DSC method is deemed to be very poorly suited for this kind of measurement because it destroys the microcapsules incorporated in the cement.

The melting latent heat is the equivalent latent heat. It reaches respectively $18528\,J.kg^{-1}$ with the power law model and $19490\,J.kg^{-1}$ with error function model, see table 5. These results are in agreement with the DSC measurements where for a mass sample of 836×10^{-3}g, the latent heat is to $16692\,J.kg^{-1}$ for melting at a heating rate of $0.1\,K.min^{-1}$. The difference between the latent heat is approximately 11% with power law and 17% with error function reported to the DSC value. Furthermore, if a mass fraction of PCM of 14.5% is taken into account, the latent heat of the PCM reaches the values $128\sim134\,kJ.kg^{-1}$ against $185\,kJ.kg^{-1}$ given by the manufacturer for pure material. In reality, the exact mass fraction of the PCM is missing because many shells are destroyed during the making process. These results suggest a mass fraction of PCM of about 10%.

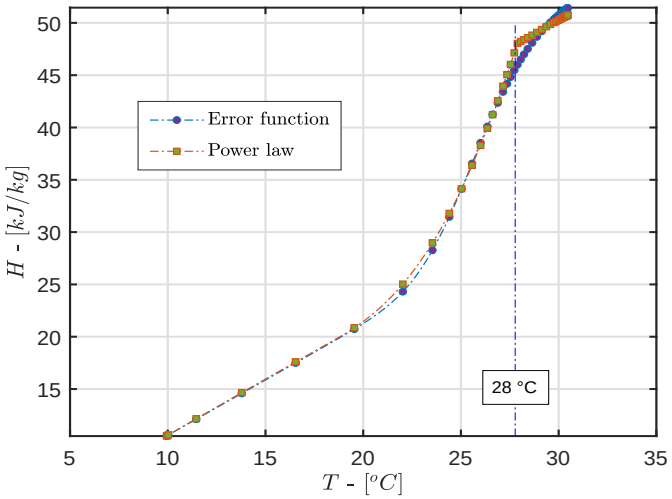

Figure 9: Enthalpy as function of temperature

The phase change temperature T_m is a medium temperature of the PCM-mortar mixture. The phase change is occurring on the temperature range $[T_m-\alpha;T_m+\alpha]$ of the PCM-mortar mixture. From the estimation results, the figure 9 shows final temperature of melting which reaches $28\,^oC$ for power law

model and 31.9 °C with error function model. The melting temperature (28 °C) of the pure PCM given by the manufacturer is completely in according to the melting temperature estimated with the power law.

7 Conclusion

The main contribution of this research work is to present the estimation of smooth function built to model the temperature dependence of effective heat capacity of a PCM undergoing solidification or melting. The estimation is conducted thanks to temperatures and heat fluxes measurements recorded carefully on the boundaries and inside the PCM sample. The enthalpy method and its variants forms (apparent specific heat and/or source method) is used to handle the phase problem resolution. Representing the phase transition by power law function was found to give better results than those obtained with error function model. The effective specific heat capacity is relatively easy to be reconstructed when a good experimental data are available inside the sample where the phase change is occurring. More sensors implemented carefully in the PCM sample should produce a better results and reduce the estimation time.

The presented method is preferred to the differential scanning method in the sense that it has the merit and the advantage of being very close to the real use conditions and dealing with a representative sample size in volume and mass. Indeed, the actual PCM sample structure and its thermal metrology allows the collection of reliable and rich information resulting from the application of any sharply varying thermal cycle on its boundaries. The method has the great advantage to works with closed eyes, i.e. it totally ignores the nature of the sample, mixing proportion of PCM in the mortar matrix, nature of the PCM, and so on. Own and precise heat fluxes and temperature measurements represent the cornerstone of this method.

Good agreements have been reached between the calculation results of the presented method and the experimental data obtained with the DSC facilities and those of literature. It demonstrates that the proposed inverse approach together with the effective heat capacity model satisfies the required accuracy and is well qualified and nicely suited for the calculation of the heat transfer process for isothermal or mushy zone phase problem.

Further numerical simulations and experimental work are needed to generalize the presented approach. This research highlights the requirement to have a reliable experimental tool for the measurement and/or estimation of the PCM thermophysical properties. Without tracking the moving phase change boundary, the enthalpy based effective heat capacity represents a simple and an accurate tool to investigate the thermal behaviour of phase change materials in different applications such as : thermal storage, aircraft cabin temperature control, building thermal management, ...

Conflict of interest

The authors declare that they have no known competing financial interests or personal relationships that could have appeared to influence the work reported in this paper.

Nomenclature

Physics variable

c	specific heat capacity $[J/kg \cdot K]$
f	liquid fraction
$g(x)$	Initial temperature $[^oC]$
h	Enthalpy $[J/kg]$
h_0	thermal conductance $[W/m^2K]$
h_ℓ	thermal conductance $[W/m^2K]$
k	thermal conductivity $[W/m \cdot K]$
ℓ	plate thickness $[m]$
L	latent heat $[kJ/kg]$
n	power exponent
N_p	number of parameters
N_s	number of sensors
N_t	number of time steps
p, q	heat flux $[W/m^2]$
S	objectif function, source term $[W/m^3]$
T	temperature $[^oC]$
t	time $[s]$
x	space $[m]$
$X_{\_}$	sensitivity coefficient $[W/m^2]$

Abbreviations

PCM	phase change material

Greek Letters

α	temperature phase change interval $[^oC]$
β_k	parameter component
β	Vector of unknowns parameters
Δ	small temperature interval
δ	small variation
ρ	density $[kg/m^3]$

Subscripts

k	component k
ℓ	at $\mathrm{x} = \ell$
l	liquid
m	melting
0	at $\mathrm{x} = 0$
p	parameter
r	reference
s	solid, sensor
t	time

References

[1] J. Crank. *Free and moving boundary problems*. Clarendon Press, Oxford, 1984.

[2] V. Alexiades and A.D. Solomon. *Mathematical modeling of melting and freezing processes*. Taylor & Francis, Washington, 1992.

[3] Saleh Nasser AL-Saadi and Zhiqiang (John) Zhai. Modeling phase change materials embedded in building enclosure: A review. *Renewable and Sustainable Energy Reviews*, 21:659–673, 2013.

[4] R. W. Lewis and K. Ravindran. Finite element simulation of metal casting. *International Journal for Numerical Methods in Engineering*, 47(1-3):29–59, 2000.

[5] H. Yang and Y. He. Solving heat transfer problems with phase change via smoothed effective heat capacity and element-free galerkin methods. *International Communications in Heat and Mass Transfer*, 37(4):385 – 392, 2010.

[6] Y. He, X. Dong, and H. Yang. A new adaptive algorithm for phase change heat transfer problems based on quadtree sbfem and smoothed effective heat capacity method. *Numerical Heat Transfer, Part B: Fundamentals*, 75(2):111–126, 2019.

[7] N.R. Eyres, D.R. Hartree, J. Ingham, R.J. Sarjant, and J.B. Wagstaff. The calculation of variable heat flow in solids. *Philosophical Transactions of the Royal Society of London, Series A, Mathematical and Physical Sciences*, 240(813):2401–57, 1946.

[8] König-Haagen A., E. Franquet, E. Pernot, and D. Brüggemann. A comprehensive benchmark of fixed-grid methods for the modeling of melting. *International Journal of Thermal Sciences*, 118:69–103, 2017.

[9] H. Nazir and *et al.* Recent developments in phase change materials for energy storage applications: A review. *International Journal of Heat and Mass Transfer*, 129:491–523, 2019.

[10] A.S. Fleischer. *Thermal Energy Storage Using Phase Change Materials, Fundamentals and Applications*. Springer, New York, 2015.

[11] X. Huang, C. Zhu, Y. Lin, and G. Fang. Thermal properties and applications of microencapsulated pcm for thermal energy storage: A review. *Applied Thermal Engineering*, 147:841–855, 2019.

[12] A. Fallahi, G. Guldentops, M. Tao, S. Granados-Focil, and S. Van-Dessel. Review on solid-solid phase change materials for thermal energy storage: Molecular structure and thermal properties. *Applied Thermal Engineering*, 127:1427–1441, 2017.

[13] R. Cheng, M. Pomianowski, X. Wang, P. Heiselberg, and Y. Zhang. A new method to determine thermophysical properties of pcm-concrete brick. *Applied Energy*, 112:988–998, 2013.

[14] M. Lachheb, Z. Younsi, H. Naji, M. Karkri, and S. Ben-Nasrallah. Thermal behavior of a hybrid pcm/plaster: A numerical and experimental investigation. *Applied Thermal Engineering*, 111:49 – 59, 2017.

[15] K. Darkwa and P.W. O'Callaghan. Simulation of phase change drywalls in a passive solar building. *Applied Thermal Engineering*, 26(8):853 – 858, 2006.

[16] A. Joulin, Z. Laurent, S. Lassue, D.R. Rousse, and J.P. Cavrot. Experimental and numerical investigation of a phase change material: Thermal-energy storage and release. *Applied Energy*, 88(7):2454–2462, 2011.

[17] A. Joulin, L. Zalewski, S. Lassue, and H. Naji. Experimental investigation of thermal characteristics of a mortar with or without a micro-encapsulated phase change material. *Applied Thermal Engineering*, 66(1):171–180, 2014.

[18] E. Franquet, S. Gibout, P. Tittelein, L. Zalewski, and J.-P. Dumas. Experimental and theoretical analysis of a cement mortar containing microencapsulated pcm. *Applied Thermal Engineering*, 73(1):30–38, 2014.

[19] L. Zalewski, E. Franquet, S. Gibout, P. Tittelein, and D. Defer. Efficient characterization of macroscopic composite cement mortars with various contents of phase change material. *Applied Sciences*, 9(6), 2019.

[20] R. Kandasamy, X.Q. Wang, and A.S. Mujumdar. Application of phase change materials in thermal management of electronics. *Applied Thermal Engineering*, 27(17-18):2822–2832, 2007.

[21] Y. Dutil, D.R. Rousse, H. Bensalah, S. Lassue, and L. Zalewski. A review on phase-change materials: Mathematical modeling and simulations. *Renewable and Sustainable Energy Reviews*, 15(1):112 – 130, 2011.

[22] L.F. Cabeza, C. Castellón, M. Nogués, M. Medrano, R. Leppers, and O. Zubillaga. Use of microencapsulated pcm in concrete walls for energy savings. *Energy and Buildings*, 39(2):113–119, 2007.

[23] T. Lee, D.W. Hawes, D. Banu, and D. Feldman. Control aspects of latent heat storage and recovery in concrete. *Solar Energy Materials and Solar Cells*, 62(3):217–237, 2000.

[24] Y. Zhang, Y. Jiang, and Y. Jiang. A simple method, the t-history method, of determining the heat of fusion, specific heat and thermal conductivity of phase-change materials. *Measurement Science and Technology*, 10(3):201–205, 1999.

[25] E.D. Kravvaritis, K.A. K A Antonopoulos, and C. Tzivanidis. Improvements to the measurement of the thermal properties of phase change materials. *Measurement Science and Technology*, 21(4):045103, 2010.

[26] E.D. Kravvariti, K.A. Antonopoulos, and C. Tzivanidis. Experimental determination of the effective thermal capacity function and other thermal properties for various phase change materials using the thermal delay method. *Applied Energy*, 88(12):4459–4469, 2011.

[27] F.A. Albouchi, M. Lachheb, M. Karkri, T. Ben-Ameur, and S. Ben-Nasrallah. Investigation of a graphite/paraffin phase change composite. *International Journal of Thermal Sciences*, 88:128–135, 2015.

[28] E. Güther, S. Hiebler, H. Mehling, and R. Redlich. Enthalpy of phase change materials as a function of temperature: Required accuracy and suitable measurement methods. *International Journal of Thermophysics*, 30:1257–1269, 2009.

[29] Y. Cascone and M. Perino. Estimation of the thermal properties of pcms through inverse modelling. *Energy Procedia*, 78:1714–1719, 2015.

[30] J.V. Beck and K.J. Arnold. *Parameter Estimation in Engineering and Sciences*. John Wiley & Sons, New York, 1977.

[31] J.V. Beck, B. Blackwell, C.R.S. Clair, and C.R.S. Clair. *Inverse Heat Conduction: Ill-Posed Problems*. Wiley-Interscience publication. Wiley, New York, 1985.

[32] M.N. Ozisik and H.R. Orlande. *Inverse Heat Transfer, Fundamentals & Applications*. Taylor & Francis, New York, 2000.

[33] O.M. Alifanov. *Inverse Heat Transfer Problems*. Springer-Verlag, Berlin Heidelberg, 1994.

[34] L. Gosselin, M. Tye-Gingras, and F. Mathieu-Potvin. Review of utilization of genetic algorithms in heat transfer problems. *International Journal of Heat and Mass Transfer*, 52(9):2169–2188, 2009.

[35] R. Derbal, D. Defer, A. Chauchois, and E. Antczak. A simple method for building materials thermophysical properties estimation. *Construction and Building Materials*, 63:197–205, 2014.

[36] K. Chaffar, A. Chauchois, D. Defer, and L. Zalewski. Thermal characterization of homogeneous walls using inverse method. *Energy and Buildings*, 78:248–255, 2014.

[37] M. Lachheb, M. Karkri, F. Albouchi, F. Mzali, and S. Ben Nasrallah. Thermophysical properties estimation of paraffin/graphite composite phase change material using an inverse method. *Energy Conversion and Management*, 82:229–237, 2014.

[38] M. Cui, X. Gao, and J. Zhang. A new approach for the estimation of temperature-dependent thermal properties by solving transient inverse heat conduction problems. *International Journal of Thermal Sciences*, 58:113–119, 2012.

[39] T. Lecompte, P. Le Bideau, P. Glouannec, D. Nortershauser, and S. Le Masson. Mechanical and thermo-physical behaviour of concretes and mortarscontaining phase change material. *Energy and Buildings*, 94:52–60, 2015.

[40] M. Hunger, A.G. Entrop, I. Mandilaras, H.J.H. Brouwers, and M. Founti. The behavior of self-compacting concrete containing micro-encapsulated phase change materials. *Cement and Concrete Composites*, 31(10):731–743, 2009.

[41] M.N. Ozisik. *Finite Difference Method in Heat Transfer*. CRC Press, Inc., Boca Raton, Florida, 1994.

[42] V.R. Voller and C.R. Swaminathan. General source-based method for solidification phase change. *Numerical Heat Transfer, Part B: Fundamentals*, 19(2):175–189, 1991.

[43] F. Rosler and Bruggemann D. Shell-and-tube type latent heat thermal energy storage: numerical analysis and comparison with experiments. *Heat Mass Transfer*, 47:1027–1033, 2011.

[44] V.R. Voller and C.R. Swaminathan. On the enthalpy method. *International Journal of Numerical Methods for Heat & Fluid Flow*, 3(3):233–244, 1993.

[45] K. Levenberg. A method for the solution of certain problems in least squares. *Quarterly of Applied Mathematics*, 2:164–168, 1944.

[46] D. Marquardt. An algorithm for least-squares estimation of nonlinear parameters. *SIAM Journal on Applied Mathematics*, 11:431–441, 1963.

[47] P.E. Gill and W. Murray. Algorithms for the solution of the nonlinear least-squares problem. *SIAM Journal on Applied Mathematics*, 15(5):977–992, 1978.

[48] *MATLAB R2017b*. MathWorks, 3 Apple Hill Dr., Natick, MA 01760, 2017.

A Analytical solution

To check its validity and capabilities, the enthalpy method developed in this paper is compared to the well known Neumann analytical solution given in reference [1, 2] as applied to melting semi-infinite slab $0 < x < \infty$ having the following thermal properties of Glauber's salt (sodium sulfate decahydrate) i.e. $\rho = 1460\,kg/m^3$, $T_m = 32\,^oC$, $L = 251.21\,kJ/kg$, $c_l = 3.31\,kJ/kg$, $c_s = 1.76\,kJ/kg$, $k_l = 0.59\,W/m^oC$ and $k_s = 2.16\,W/m^oC$. Initially, the solid is at a uniform temperature $T(x,0) = T_i = 25\,^oC$ that is lower than the phase change temperature T_m. At time $t > 0$, the temperature of the boundary surface $x = 0$ is suddenly raised to a temperature $T_0 = 90\,^oC$, which is higher than the melting temperature T_m and maintained at that temperature for $t > 0$.

The Neumann solution of the two-phase Stefan problem described above is given by :

- Melting interface location:

$$X(t) = 2\lambda\sqrt{\alpha_l t}, \qquad t > 0$$

- Temperature in the liquid region, i.e. $0 < x < X(t)$ for $t > 0$ is given by

$$T(x,t) = T_0 - (T_0 - T_m)\,\mathrm{erf}\Big(\frac{x}{2\sqrt{\alpha_l t}}\Big)\Big/\mathrm{erf}(\lambda)$$

- Temperature in the solid region, i.e. $x > X(t)$ for $t > 0$ is given by

$$T(x,t) = T_i + (T_m - T_i)\,\mathrm{erfc}\Big(\frac{x}{2\sqrt{\alpha_s t}}\Big)\Big/\mathrm{erfc}(\nu\lambda)$$

Here λ is the solution of the transcendental equation

$$\frac{St_l}{\exp(\lambda^2)\mathrm{erf}(\lambda)} - \frac{St_s}{\nu\exp(\nu^2\lambda^2)\mathrm{erfc}(\nu\lambda)} = \lambda\sqrt{\pi}$$

with the two Stefan numbers St_s, St_l and parameter ν defined by

$$St_l = \frac{c_l(T_0 - T_m)}{L}, \qquad St_s = \frac{c_s(T_m - T_i)}{L}, \qquad \nu = \sqrt{\frac{\alpha_l}{\alpha_s}}$$

From the given thermal properties, one can easily compute the following properties : $\alpha_s = 8.41 \times 10^{-7}\,m^2/s$, $\alpha_l = 1.22 \times 10^{-7}\,m^2/s$, $\nu = 0.381$, $St_s = 0.049$, $St_l = 0.764$ and the root of the transcendental equation $\lambda = 0.520$.

Figure 10 shows the comparison between analytical and numerical temperature profiles at different space and time locations. For the presented test case, results of the power law model match fairly both space and time analytical profiles. The enthalpy method coupled with the power law seems to give better results than the erf law and approximates correctly the phase change undergone by the material.

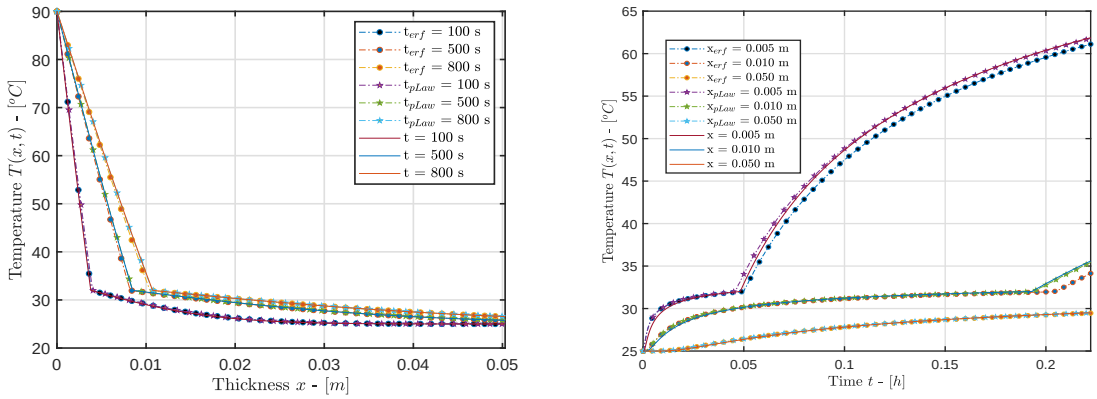

(a) Temperatures as function of space

(b) Temperatures as function of time

Figure 10: Comparison between analytical and numerical temperature profiles for both used enthalpy-temperature model : erf function and power law